

# Electronic band structure and carrier effective mass in calcium aluminates

Julia E. Medvedeva,\* Emily N. Teasley, and Michael D. Hoffman  
*Department of Physics, University of Missouri–Rolla, Rolla, MO 65409*

First-principles electronic band structure investigations of five compounds of the CaO-Al<sub>2</sub>O<sub>3</sub> family, 3CaO·Al<sub>2</sub>O<sub>3</sub>, 12CaO·7Al<sub>2</sub>O<sub>3</sub>, CaO·Al<sub>2</sub>O<sub>3</sub>, CaO·2Al<sub>2</sub>O<sub>3</sub> and CaO·6Al<sub>2</sub>O<sub>3</sub>, as well as CaO and  $\alpha$ -,  $\theta$ - and  $\kappa$ -Al<sub>2</sub>O<sub>3</sub> are performed. We find that the conduction band in the complex oxides is formed from the oxygen antibonding  $p$ -states and, although the band gap in Al<sub>2</sub>O<sub>3</sub> is almost twice larger than in CaO, the  $s$ -states of *both* cations. Such a hybrid nature of the conduction band leads to isotropic electron effective masses which are nearly the same for all compounds investigated. This insensitivity of the effective mass to variations in the composition and structure suggests that upon a proper degenerate doping, both amorphous and crystalline phases of the materials will possess mobile extra electrons.

**PACS number(s):** 71.20.-b

## Introduction

Oxides of the main group metals such as CaO and Al<sub>2</sub>O<sub>3</sub> are known for their superior refractory properties and until recently these materials seemed to be inappropriate choice to serve as electrical conductors. Hence, the discovery [1] of an insulator-conductor conversion in 12CaO·7Al<sub>2</sub>O<sub>3</sub> (12C7A or mayenite), a member of Portland cements, generated a lot of excitement and fueled the quest for new directions towards inexpensive and environmentally friendly materials for (opto)electronic applications.

The remarkable electrical properties of 12CaO·7Al<sub>2</sub>O<sub>3</sub> – currently, conductivities as high as 1700 S/cm were achieved [2, 3] and various insulator-to-metal conversion approaches were employed [1, 2, 3, 4, 5, 6, 7] – originate from its unique structural feature, namely, the presence of so-called “free” oxygen ions located inside spacious cages of  $\sim 5.6$  Å in diameter. Introduction of other charge-balance ions (H<sup>-</sup>, OH<sup>-</sup>, Cl<sup>-</sup>, F<sup>-</sup>) into the cages or their reduction leads to a wide range of semiconducting to metallic behavior which can be controlled via the concentration of these ions. Accurate band structure calculations have revealed the origin of the observed unusual phenomena and also allowed predictions of ways to vary the conductivity over several orders of magnitude [6, 8, 9, 10]. Furthermore, it was demonstrated [11] that 12CaO·7Al<sub>2</sub>O<sub>3</sub> is the first of a conceptually new class of transparent conductors where the structural peculiarities and the resulting electronic band structure features suggest an approach to achieve good electrical conductivity without compromising their optical properties – the bottleneck in conventional transparent conducting oxides [11, 12].

In this work we focus on the structural, electronic and optical properties of the other four members of the CaO-Al<sub>2</sub>O<sub>3</sub> family – 3CaO·Al<sub>2</sub>O<sub>3</sub> (3CA), CaO·Al<sub>2</sub>O<sub>3</sub> (CA), CaO·2Al<sub>2</sub>O<sub>3</sub> (C2A or grossite) and CaO·6Al<sub>2</sub>O<sub>3</sub> (C6A or hibonite) – and compare with those of 12C7A, CaO and  $\alpha$ -,  $\theta$ - and  $\kappa$ -Al<sub>2</sub>O<sub>3</sub>. Based on the results of the

first-principles density functional investigations, we find that despite variations in the composition and structural diversity in these calcium aluminate compounds, their electron effective masses are nearly the same and are isotropic. The later suggests that isotropic character of the electron transport can be achieved upon proper carrier generation in these complex multi-cation oxides. We compare the electronic band structure features of calcium aluminates with those of the conventional transparent conducting oxides (TCO) and discuss the advantages of CaO-Al<sub>2</sub>O<sub>3</sub> compounds as candidates for novel TCO hosts.

## Crystal structure

Calcium aluminates (also known as high alumina cements) have a rich phase diagram which includes five lime-alumina compounds – 3CA, 12C7A, CA, C2A and C6A [13, 14, 15, 16, 17, 18, 19, 20, 21, 22, 23]. Among them, 12C7A has the lowest melting point (1722 °C) and C6A has the highest (2156 °C) which is comparable to the one of pure alumina (2327 °C). Such a superior refractory properties of these materials make them attractive for various applications as ceramics and glasses as well as in cement and steel industries [24, 25]. Calcium aluminates have been grown by several techniques including solid state reactions (sintering), sol-gel technologies and self-propagating combustion synthesis, see [22, 23, 24] and references therein.

CaO-Al<sub>2</sub>O<sub>3</sub> family has two cubic, two monoclinic and one hexagonal structure. Table I lists the lattice space groups of the compounds along with the number of formula units in the unit cell (used in our band structure calculations), the average cation-anion distances and oxygen coordination of the cations. Calcium aluminates exhibit a variety of structural peculiarities. The above mentioned 12C7A with nanoporous cages has loosely bound oxygen O<sup>2-</sup> ions inside two out of the total 12 cages (in the conventional unit cell). These “free” anions can be easily substituted with F<sup>-</sup>, Cl<sup>-</sup> or OH<sup>-</sup> [26, 27, 28, 29] or re-

duced [5]. In addition, aliovalent substitution of  $\text{Al}^{3+}$  with  $\text{Si}^{4+}$  results in an increase of the number of the free oxygen ions and in the formation of oxygen radicals such as  $\text{O}_2^-$  and  $\text{O}_2^{2-}$  inside the cages [10, 30]. Tricalcium aluminate, 3CA, consists of six-fold rings of  $\text{AlO}_4$  tetrahedra surrounding structural voids of 1.5 Å in diameter; Ca ions join these rings together [31]. In calcium hexaluminate, C6A, there are double layers of pure  $\text{AlO}_4$  and “penta-coordinated”  $\text{Al}^{3+}$  ions which are displaced from the trigonal pyramidal site center [32, 33, 34]. These structural peculiarities may result in specific features in the electronic band structure and also may suggest possible ways for efficient carrier generation. For example, empty spaces can serve as sites for dopants or guest atoms. Atoms from the structurally distinct layers or with unusual coordination may facilitate a defect formation or may be the target for substitutional doping. Ions that are loosely bound to the host framework can be easily reduced to provide extra electrons which balance the charge neutrality and so may lead to electrical conductivity.

### Methods

The electronic band structure calculations of calcium aluminates were performed using two density functional methods within the local density approximation. First, the linear muffin-tin orbital method (LMTO) in the atomic sphere approximation [35] was employed. For these calculations, lattice parameters and atomic positions were fixed to the experimental values (3CA [31], 12C7A [36], CA [37], C2A [38], C6A [32], monoclinic  $\theta$ - $\text{Al}_2\text{O}_3$  [39] and orthorhombic  $\kappa$ - $\text{Al}_2\text{O}_3$  [40]). The muffin-tin radii are 3.0-4.0 a.u. for Ca, 1.9-2.3 a.u. for Al and 1.7-2.2 a.u. for O atoms. Because these structures are not closely packed, we included 2, 320, 85, 84, 40, 70, 8, 23 and 44 empty spheres to fill the open space in CaO, 3CA, 12C7A, CA, C2A, C6A,  $\alpha$ - $\text{Al}_2\text{O}_3$ ,  $\theta$ - $\text{Al}_2\text{O}_3$  and  $\kappa$ - $\text{Al}_2\text{O}_3$  structure, respectively. The number of irreducible  $\mathbf{k}$ -points in the Brillouin zone was in the range of 11-170 points.

In addition, we employed the highly-precise full-potential linearized augmented plane-wave (FLAPW) method [41, 42] to calculate accurately the atomic contributions to the conduction band wavefunctions in CaO, 12C7A, C2A, C6A and  $\text{Al}_2\text{O}_3$ . 3CA and CA were not included in these studies because of the large number of atoms in their unit cells, 264 and 84, respectively, which makes the calculations computationally challenging. For each structure investigated within FLAPW method, the internal positions of all atoms have been optimized via the total energy and atomic forces minimization, while the lattice parameters were fixed at the experimental values. For the FLAPW calculations cutoffs for the basis functions, 16.0 Ry, and potential representation, 81.0 Ry,

and expansion in terms of spherical harmonics with  $\ell \leq 8$  inside the muffin-tin spheres were used. The muffin-tin radii were 2.6 a.u. for Ca, 1.7 for Al and 1.5 for O atoms. Summations over the Brillouin zone were carried out using 10-19 special  $\mathbf{k}$  points in the irreducible wedge.

### Electronic band structure

The electronic band structures calculated along the high-symmetry directions in the corresponding Brillouin zones of the calcium aluminates are shown in Fig. 1. All plots have the same energy scale so that the increase in the band gap value as the CaO ( $\text{Al}_2\text{O}_3$ ) content decreases (increases), i.e., in the order  $\text{C} < 3\text{CA} < 12\text{C7A} < \text{CA} < \text{C2A} < \text{C6A} < \alpha\text{-A}$ , is clearly seen. Table I lists the band gap and the valence band width (VBW) which also increases for the compounds with higher alumina content. The largest VBW value is found for the hexagonal C6A which has higher crystal symmetry and hence provides the larger overlap between the orbitals of the neighboring atoms – compared to those of the pure alumina phases (rhombohedral, monoclinic or orthorhombic, Table I).

As expected, LDA underestimates the band gap in all oxides. Our calculated band gap values are smaller by at least 1.45 eV for CaO (for the direct band gap at  $\Gamma$  point), by 0.8 eV for C12A7 and by 2.3 eV for  $\alpha$ - $\text{Al}_2\text{O}_3$  as compared to the available experimental optical data. The obtained band gaps are similar to the LDA results reported earlier for CaO [43, 44, 45] and  $\alpha$ - $\text{Al}_2\text{O}_3$  [46]. Note that the band gap underestimation does not affect the conclusions made.

It is widely accepted that the conduction band(s) in oxides of the main group metals is formed from the cations states, i.e., Ca  $s$  and  $d$  and Al  $s$  and  $p$  states. However, our detailed analysis of the wavefunctions at the bottom of the conduction band, Table II, provides a different picture: we find that the oxygen antibonding  $p$ -states give similar contributions as compared to those from the cation(s)  $s$ -states [47]. Further, we find that the relative atomic contributions are similar within the room-temperature energy range, i.e., within  $\sim 30$  meV above the bottom of the conduction band. Thus, both the cation(s)  $s$  and anion  $p$  states will be available for the transport of extra carriers and hence will determine the electron mobility in these materials once they are degenerately doped.

It is important to point out that the density of states at the bottom of the conduction band is low due to the high dispersion  $E(k)$  in this energy range which in turn originates in the large overlap between the wavefunctions of the neighboring cations and anions, i.e., the spherically symmetric  $s$ -orbitals and  $p$ -orbitals of the oxygen atoms. As discussed below, the low density of states will ensure the desired low optical absorption in degenerately doped materials. Calcium  $d$  and aluminum  $p$  states give a sig-

nificantly larger contributions to the density of states; however, because these states are located at much higher energies, they will not be available for charge transport.

Another counter-intuitive finding is that the Ca and Al states give comparable contributions to the bottom of the conduction band in these binary compounds. This may come as a surprise because the band gap in  $\text{Al}_2\text{O}_3$  is almost twice larger than the one in CaO, and so the unoccupied Al  $s$ -states are expected to be located deep in the conduction band. Based on the analysis of the wavefunction at the bottom of the conduction band in several CaO- $\text{Al}_2\text{O}_3$  compounds calculated within highly precise FLAPW method, we find that the contributions from Al atoms are not negligible in 12C7A, C2A and C6A, Table II. Therefore, the states of *both* cations – as well as the oxygen antibonding states – will be available for extra electrons in properly doped materials. Such a hybrid nature of the conduction band may lead to a three-dimensional (isotropic) network for the electron transport in these complex multi-cation oxides – that is consistent with the isotropic electron effective masses reported below.

### Electron effective mass

Since the states of Ca and Al give comparable contributions to the conduction states in calcium aluminate oxides, both should contribute to the electron effective mass. Hence, for each binary compound one may expect an “effective” average over the effective masses of lime and alumina [51]. This may appear to be similar to the linear interpolation of the band gap and the electron effective mass within the virtual crystal approximation (VCA) that has been known and widely utilized for semiconductor alloys, such as  $\text{Ga}_{1-x}\text{In}_x\text{As}$  or  $\text{Ga}_{1-x}\text{Al}_x\text{N}$ . For alloys, however, the crystal lattice remains the same as the concentration of constituents is varied via substitution. In contrast, in calcium aluminates, the band gap and the effective mass averaging (which follows from VCA) is not justified because the lattice structure in these compounds is dramatically different from the structure of the terminal phases. Moreover, in all binary compounds with the exception for C6A, Al atoms have four oxygen neighbors while there is no alumina compound where all cations are 4-coordinated, Table I. Nevertheless, the increase in both the band gap and the electron effective mass as the content of  $\text{Al}_2\text{O}_3$  increases is clearly seen from Table I.

We point out here that the electron effective mass is directly related to the band gap value according to the  $\mathbf{k}\cdot\mathbf{p}$  theory, namely, the smaller the band gap, the smaller the electron effective mass and vice versa [52]. However, the electron effective mass also depends on the overlap between the wavefunctions of the neighboring atoms, i.e., between the cation  $s$ -orbitals and the antibonding

$p$ -orbitals of the oxygen atoms. Therefore, in addition to the oxygen coordination, the distortions in the polyhedra and in the cation-anion chains affect the orbital overlap and, hence, the electron effective mass. This explains the fact that the effective mass is lower in orthorhombic  $\kappa$ - $\text{Al}_2\text{O}_3$  than in monoclinic alumina phase despite the opposite trend in the band gaps, Table I. These two alumina phases can be compared to C6A where both four- and six-coordinated Al atoms are also present. In the latter, the electron effective mass is the lowest due to the highest symmetry of its crystal structure which provides the largest orbital overlap.

Note that CaO has indirect band gap with the conduction band minimum at  $X$  point and the valence band maximum at  $\Gamma$  point. The electron effective masses given in Table I are calculated in the [100], [010] and [001] directions at  $\Gamma$  point. For the directions in the standard Brillouin zone, i.e., [111] or  $\Gamma L$  and [011] or  $\Gamma K$ , the electron effective masses are the same,  $0.33 m_e$ . Thus, the effective mass is isotropic at  $\Gamma$  point since the conduction band is parabolic at the wavevector  $\vec{k}=0$ , as expected. However, because  $\Gamma$  point is  $\sim 1$  eV higher in energy with respect to the bottom of the conduction band, the mobility of extra electrons will be determined by their effective mass at the  $X$  point which we find to be  $1.22 m_e$  along the  $\Gamma X$  direction.

Significantly, the electron effective mass remains nearly isotropic in all CaO- $\text{Al}_2\text{O}_3$  compounds, Table I, despite the structural complexity in these materials, namely, the low symmetry and thus local distortions in the cation-anion polyhedra; structural anisotropy due to irregular atomic arrangements such as layers, rings, or chains of one type of cations; or the presence of large structural voids. The largest deviation of the in-plane effective mass from the one calculated along the  $z$  direction is found in monoclinic  $\theta$ - $\text{Al}_2\text{O}_3$  where the anisotropy factor  $\delta = (m_e^{[100]} + m_e^{[010]})/2m_e^{[001]} - 1$  is 0.11. This finding is important from technological point of view. The isotropy of the electronic properties, i.e., the insensitivity of the electron effective mass to the oxygen coordination and structural variations, suggests that similar electronic properties can be achieved in a structure where the stoichiometry is maintained and the cations and anions alternate, i.e., cations are coordinated with anions and vice versa. Therefore, amorphous phases of calcium aluminates (which are readily available via the liquid solution, or sol-gel, preparation techniques [19, 21, 22]) can be successfully utilized. This is in marked contrast to amorphous Si where the directional interactions between the conduction  $p$ -orbitals give rise to a strong anisotropy of the transport properties and a significant decrease in the conductivity [53].

Finally, the conduction band topology in calcium aluminates resembles the one of the conventional [11] transparent conducting oxide hosts [12, 50, 54, 55, 56, 57, 58]: the high energy dispersion at the bottom of the conduc-

tion band indicates a small electron effective mass and hence should lead to a high carrier mobility upon degenerate doping of the materials. The electron effective masses found for the CaO-Al<sub>2</sub>O<sub>3</sub> compounds are comparable to those in the well-known and commercially utilized transparent conductor hosts such as In<sub>2</sub>O<sub>3</sub> (0.17  $m_e$  as obtained from an additional calculation within LMTO method for direct comparison) and ZnO (0.21  $m_e$  along the [100] and [010] directions and 0.19  $m_e$  along the [011] direction for the hexagonal phase, also calculated within LMTO). Note that the mobility of extra carriers should play a crucial role in providing good electrical conductivity because large carrier concentrations (which may be challenging to achieve in the calcium aluminate oxides [59, 60, 61]) should be avoided to keep optical absorption low. The absorption arises due to the transitions from the conduction band partially occupied by introduced electrons and due to the plasma frequency of the free carriers. In addition, currently known conventional transparent conductors (oxides of post-transition metals such as In, Zn, Sn, Ga and Cd) possess a relatively small band gaps of  $\sim 2$ -3 eV. Therefore, large carrier concentrations may be required to provide the desired optical transmittance in the short-wavelength range of the visible part of the spectrum that is attained via a pronounced displacement of the Fermi energy (so-called Burstein-Moss shift). This may not be required in calcium aluminates where significantly larger band gaps will ensure that the intense transitions from the valence band are out of the visible range.

### Hole effective mass

The electronic band structure plots, Fig. 1, reveal another interesting peculiarity, namely, the large anisotropy of the top of the valence band and, hence, of the hole effective mass, Table I. The anisotropy factor, calculated as  $\delta = (m_h^{[100]} + m_h^{[010]})/2m_h^{[001]}$ , is equal to 10.71, 0.05 and 11.83 for C2A and for monoclinic ( $\theta$ ) and orthorhombic ( $\kappa$ ) Al<sub>2</sub>O<sub>3</sub>, respectively. The large anisotropy is also observed for CA and C6A, however, we could not determine the hole effective masses in all three directions due to the non-dispersive character of the bands along some of the directions in these compounds, Table I. Small values of the hole effective mass obtained for C2A and C6A, i.e., 0.6-0.7  $m_e$ , should stimulate the search for efficient ways to convert these oxides into highly desirable p-type conductors with mobile carriers – a complementary characteristic to the n-type behavior discussed above.

### Conclusions

Based on the electronic band structure investigations of calcium aluminates with different composition and

structure, we find that anions and both cations give comparable contributions to the conduction states that may lead to isotropic three-dimensional distribution of the conduction electron density if these materials are properly doped. It is important to note, however, that doping of a structurally anisotropic material (such as 3CA, C6A or C2A) may result in a non-uniform distribution of carrier donors such as oxygen defects or aliovalent substitutional dopants. Therefore, whether or not the isotropic behavior of the host material is maintained will depend on the carrier generation mechanism. Amorphous counterparts of the cement phases readily offer a way to attain isotropic transport. In addition, due to the low electron effective mass which is shown to be insensitive to structural distortions and disorder, extra carriers in the amorphous oxides are expected to be nearly as mobile as they are in the crystalline phases, making the materials attractive from the technological point of view.

---

\* E-mail:juliaem@umr.edu

- [1] K. Hayashi, S. Matsuishi, T. Kamiya, M. Hirano, H. Hosono, *Nature* **419**, 462 (2002).
- [2] M. Bertoni, Ph.D. Thesis, Northwestern University, Evanston, IL, USA, 2006.
- [3] S.W. Kim, S. Matsuishi, T. Nomura, Y. Kubota, M. Takata, K. Hayashi, T. Kamiya, M. Hirano, and H. Hosono, *Nano Lett.* **7**, 1138 (2007).
- [4] Y. Toda, S. Matsuishi, K. Hayashi, K. Ueda, T. Kamiya, M. Hirano, and H. Hosono, *Adv. Mater.* **16**, 685 (2004).
- [5] S. Matsuishi, Y. Toda, M. Miyakawa, K. Hayashi, T. Kamiya, M. Hirano, I. Tanaka, and H. Hosono, *Science* **301**, 626 (2003).
- [6] J.E. Medvedeva, A.J. Freeman, M.I. Bertoni, T.O. Mason, *Phys. Rev. Lett.* **93**, 16408 (2004)
- [7] S.W. Kim, M. Miyakawa, K. Hayashi, T. Sakai, M. Hirano, and H. Hosono, *J. Amer. Chem. Soc.* **127**, 1370 (2005); S.W. Kim, Y. Toda, K. Hayashi, M. Hirano, and H. Hosono, *Chem. Mater.* **18**, 1938 (2006); S.W. Kim, K. Hayashi, M. Hirano, H. Hosono, and I. Tanaka, *J. Amer. Ceram. Soc.* **89**, 3294 (2006).
- [8] J.E. Medvedeva, A.J. Freeman, *Appl. Phys. Lett.* **85**, 955 (2004).
- [9] M.I. Bertoni, T.O. Mason, J.E. Medvedeva, A.J. Freeman, K.R. Poeppelmeier, B. Delley, *J. Appl. Phys.* **97**, 103713 (2005).
- [10] M. Bertoni, J.E. Medvedeva, Y.Q. Wang, A. Freeman, K.R. Poeppelmeier, and T.O. Mason, *J. Appl. Phys.*
- [11] J.E. Medvedeva, A.J. Freeman, *Europhys. Lett.* **69**, 583 (2005).
- [12] J.E. Medvedeva, *Appl. Phys. A* (2007).
- [13] E.S. Shepherd, G.A. Rankin, and F.E. Wright, *Am. J. Sci.* **28**, 293 (1909); G.A. Rankin, and F.E. Wright, *Am. J. Sci.*, **39**, 1 (1915).
- [14] L.G. Wisnyi, *The High Alumina Phases in the System Lime-Alumina*, Ph.D. Thesis, Rutgers University, New Brunswick, NJ, USA, 1955.
- [15] *Structure and performance of cements*, edited by P. Barnes (Applied Science Publishers, 1983).

- [16] L.P. Morozova, F.D. Tamas, and T.V. Kuznetsova, *Cement and Concrete Research* **18**, 375 (1988).
- [17] B. Hallstedt, *J. Am. Cer. Soc.* **73**, 15 (1990).
- [18] V.K. Singh, M.M. Ali, and U.K. Mandal, *J. Amer. Ceram. Soc.* **73**, 872 (1990).
- [19] A.A. Goktas, and M.C. Weinberg, *J. Am. Ceram. Soc.* **74**, 1066 (1991).
- [20] G. Eriksson, and A.D. Pelton, *Metall. Trans. B* **24B**, 807 (1993).
- [21] M.A. Gulgun, O.O. Popoola, W.M. Kriven, *J. Am. Ceram. Soc.* **77**, 531 (1994).
- [22] A.C. Tas, *J. Amer. Ceram. Soc.* **81**, 2853 (1998).
- [23] H.C. Yi, J.Y. Guigné, J.J. Moore, F.D. Schowengerdt, L.A. Robinson, and A.R. Manerfino, *J. Mater. Science* **37**, 4537 (2002).
- [24] J.E. Kopanda, and G. Mac Zura, *Alumina Chemicals Science and Technology Handbook*, edited by L.D. Hart (American Ceramic Society, Westerville, OH, 1990), p. 171.
- [25] J.E. Shelby, C.M. Shaw, and M.S. Spess, *J. Appl. Phys.* **66**, 1149 (1989).
- [26] J. Jeevaratnam, F.P. Glasser, and L.S. Dent Glasser, *J. Am. Ceram. Soc.* **47** 105 (1964).
- [27] A.K. Chatterjee, and G.I. Zhmoidin, *J. Mater. Sci.* **7**, 93 (1972).
- [28] P.P. Williams, *Acta Cryst.* **B29**, 1550 (1973).
- [29] G.I. Zhmoidin, and G.S. Smirnov. *Inorganic Mater.* **18**, 1595 (1982).
- [30] S. Fujita, K. Suzuki, M. Ohkawa, T. Mori, Y. Iida, Y. Miwa, H. Masuda, and S. Shimada, *Chem. Mater.* **15**, 255 (2003); S. Fujita, M. Ohkawa, K. Suzuki, H. Nakano, T. Mori, and H. Masuda, *Chem. Mater.* **15** 4879 (2003).
- [31] P. Mondal, and J.W. Jeffery. *Acta Cryst.* **B31**, 689 (1975).
- [32] A. Utsunomiya, K. Tanaka, H. Morikawa, F. Marumo, and H. Kojima, *J. Solid State Chem.* **75**, 197 (1988).
- [33] L.-S. Du, and J.F. Stebbins, *J. Phys. Chem.* **108**, 3681 (2004).
- [34] A.M. Hofmaister, B. Wopenka, and A.J. Locock, *Geochimica et Cosmochimica Acta* **68**, 4485 (2004).
- [35] O. K. Andersen, O. Jepsen, M. Sob, *Electronic Band Structure and its Applications*, (ed. M. Yussouff. Springer-Verlag, Berlin, 1986).
- [36] A.N. Christensen. *Acta Chemica Scandinavica* **A41**, 110 (1987).
- [37] W. Hörkner, and H.K. Müller-Buschbaum, *J. Inorg. Nucl. Chem.* **38**, 983 (1976).
- [38] D.W. Goodwin, and A.J. Lindop, *Acta Cryst. B* **26**, 1230 (1970).
- [39] E. Husson E, and Y. Repelin, *Euro. J. Solid State Inorg. Chem.* **33** 1223 (1996).
- [40] B. Ollivier, R. Retoux, P. Lacorre, D. Massiot, and G. Ferey, *J. Mater. Chem.* **7** 1049 (1997).
- [41] E. Wimmer, H. Krakauer, M. Weinert, A.J. Freeman, *Phys. Rev. B* **24**, 864 (1981)
- [42] M. Weinert, E. Wimmer, A.J. Freeman, *Phys. Rev. B* **26**, 4571 (1982)
- [43] S.K. Medeiros, E.L. Albuquerque, F.F. Maia Jr, J.S. de Sousa, E.W.S. Caetano, and V.N. Freire, *J. Phys. D: Appl. Phys.* **40**, 1655 (2007).
- [44] A. Yamasaki, T. Fujiwara, *Phys. Rev. B* **66**, 245108 (2002).
- [45] H. Baltache, R. Khenata, M. Sahnoun, M. Driz, B. Abbar, and B. Bouhafs, *Physica B* **344**, 334 (2004).
- [46] A.A. Demkov, L.R.C. Fonseca, E. Verret, J. Tomfohr, and O.F. Sankey, *Phys. Rev. B* **71**, 195306 (2005).
- [47] The presence of the oxygen  $p$ -states in the conduction band of MgO and MgS has been pointed out by de Boer and de Groot [48]. A detailed comparison with CaO and CaS was later done by Basalaev *et al* [49] who found that the energy location of the unoccupied  $d$  and  $p$  states of cations affects the relative anion-cation contributions. The role of the antibonding oxygen states in the conduction states of a variety of main group oxides has been also stressed by Mizoguchi and Woodward [50].
- [48] P.K. de Boer, R.A. de Groot, *J. Phys. Condens. Matter* **10**, 10241-10248 (1998).
- [49] Y.M. Basalaev, Y.N. Zhuravlev, A.V. Kosobutskii, and A.S. Poplavnoi, *Phys. Solid State* **46**, 848 (2004).
- [50] H. Mizoguchi, and P.M. Woodward, *Chem. Mater.* **16**, 5233 (2004).
- [51] J.E. Medvedeva, *Europhys. Lett.* **78**, 57004 (2007).
- [52] This also implies that because LDA underestimates the band gap values, the electron effective masses are also underestimated.
- [53] K. Nomura, H. Ohta, A. Takagi, T. Kamiya, M. Hirano, and H. Hosono, *Nature*, **432**, 488 (2004).
- [54] A.J. Freeman, K.R. Poeppelmeier, T.O. Mason, R.P.H. Chang, and T.J. Marks, *MRS Bull.* **25**, 45 (2000).
- [55] O.N. Mryasov and A.J. Freeman, *Phys. Rev. B* **64**, 233111 (2001).
- [56] R. Asahi, A. Wang, J. R. Babcock, N. L. Edleman, A. W. Metz, M. A. Lane, V. P. Dravid, C. R. Kannewurf, A. J. Freeman, and T. J. Marks, *Thin Solid Films* **411**, 101 (2002).
- [57] Y. Yang, S. Jin, J.E. Medvedeva, J.R. Ireland, A.W. Metz, J. Ni, M.C. Hersam, A.J. Freeman, and T.J. Marks, *J. Amer. Chem. Soc.* **127**, 8796 (2005).
- [58] J.E. Medvedeva, *Phys. Rev. Lett.* **97**, 086401 (2006).
- [59] G.F. Neumark, *Mater. Sci. Eng. R* **21**, 1 (1997).
- [60] C.G. Van de Walle, *Phys. Stat. Solidi B* **229**, 221 (2002).
- [61] A. Zunger, *Appl. Phys. Lett.* **83**, 57 (2003).

	Space group	Z	$\langle D_{\text{Ca-O}} \rangle$	Ca n.n.	$\langle D_{\text{Al-O}} \rangle$	Al n.n.	$E_g$	VBW	$m_e^{[100]}$	$m_e^{[010]}$	$m_e^{[001]}$	$m_h^{[100]}$	$m_h^{[010]}$	$m_h^{[001]}$
C	$Fm\bar{3}m$	1	2.40	6	—	—	3.55	2.8	0.33	0.33	0.33	1.25	1.25	1.25
3CA	$Pa\bar{3}$	24	2.42	6	1.75	4	3.86	3.5	0.33	0.33	0.33	$\infty$	$\infty$	$\infty$
12C7A	$I\bar{4}3d$	1	2.43	6	1.75	4	4.23	5.4	0.37	0.37	0.37	2.54	2.54	2.54
CA	$P2_1/n$	12	2.51	6	1.75	4	4.53	5.0	0.39	0.38	0.37	$\infty$	3.10	$\infty$
C2A	$C2/c$	2	2.39	5	1.76	4	4.87	5.6	0.38	0.38	0.40	6.64	6.64	0.62
C6A	$P6_3/mmc$	2	2.71	6	1.80, 1.93, 1.91	4, 5, 6	5.38	7.8	0.34	0.34	0.31	0.68	0.68	$\infty$
$\alpha$ -A	$R\bar{3}c$	2	—	—	1.91	6	6.48	7.1	0.38	0.38	0.38	3.99	3.99	3.99
$\theta$ -A	$C2/m$	2	—	—	1.77, 1.93	4, 6	4.95	6.4	0.41	0.41	0.37	0.64	0.64	13.68
$\kappa$ -A	$Pna2_1$	8	—	—	1.77, 1.94	4, 6	5.49	6.6	0.37	0.35	0.36	4.90	6.22	0.47

TABLE I: Structural and electronic properties of the CaO-Al<sub>2</sub>O<sub>3</sub> compounds. Crystal space group; the number of formula units per unit cell, Z, used in the calculations; the average cation-anion distances,  $\langle D_{\text{Ca-O}} \rangle$  and  $\langle D_{\text{Al-O}} \rangle$ , in Å; the number of nearest oxygen neighbors for Ca and Al atoms, n.n.; band gap,  $E_g$ , in eV; valence band width, VBW, in eV; and the electron and hole effective masses,  $m_e$  and  $m_h$ , in units of the electron mass, calculated along the specified crystallographic directions.

Compound	$C_{\text{Ca}}^\Gamma$	$C_{\text{Al}}^\Gamma$	$C_{\text{O}}^\Gamma$
CaO	59	—	41
12CaO·7Al <sub>2</sub> O <sub>3</sub>	64	7	29
CaO·2Al <sub>2</sub> O <sub>3</sub>	49	16	34
CaO·6Al <sub>2</sub> O <sub>3</sub>	42	25	33
$\alpha$ -Al <sub>2</sub> O <sub>3</sub>	—	55	45

TABLE II: Relative average atomic contributions to the conduction band wavefunction at  $\Gamma$  point, in per cent, as calculated for several oxides within FLAPW method.

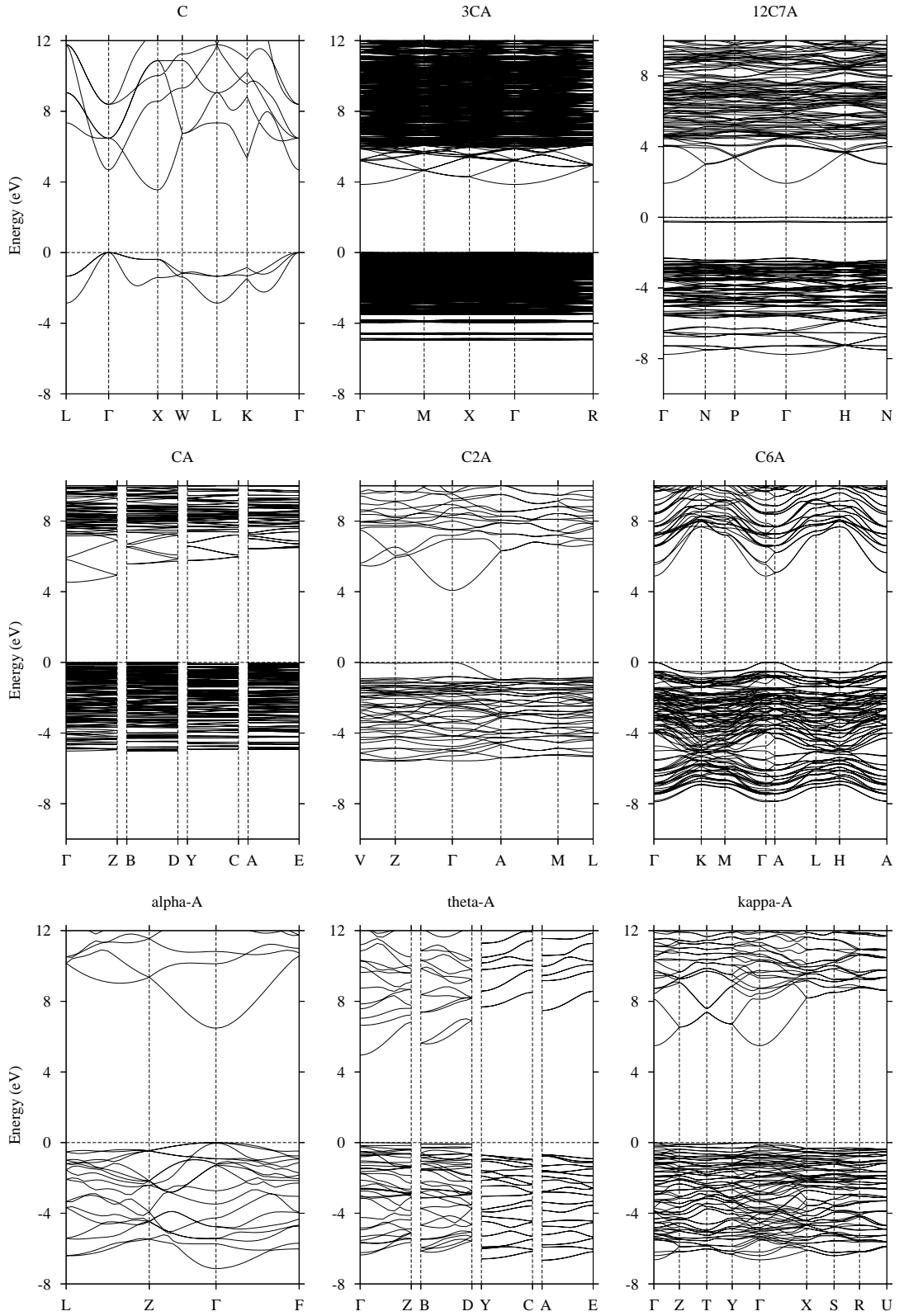


FIG. 1: Electronic band structure plots for the compounds of the  $\text{CaO-Al}_2\text{O}_3$  family and the terminal phases,  $\text{CaO}$  and  $\alpha\text{-Al}_2\text{O}_3$ . Band structures of monoclinic  $\theta\text{-Al}_2\text{O}_3$  and orthorhombic  $\kappa\text{-Al}_2\text{O}_3$  are given for comparison.